ISSN 0010-5082, Combustion, Explosion, and Shock Waves, 2021, Vol. 57, No. 3, pp. 356–363. © Pleiades Publishing, Ltd., 2021.

Detonation of Ultrafine Explosives

A. P. Ershov[a], V. V. Andreev[a], A. O. Kashkarov[a], Ya. L. Luk'yanov[a], D. A. Medvedev[a], E. R. Pruuel[a], I. A. Rubtsov[a], N. P. Satonkina[a], and S. A. Solov'ev[b]

UDC 662.215.1

Published in *Fizika Goreniya i Vzryva*, Vol. 57, No. 3, pp. 111–118, May–June, 2021.
Original article submitted June 1, 2020; revision submitted July 30, 2020; accepted for publication July 31, 2020.

Abstract: Detonation of PETN and HMX with a particle size of about 1 μm was investigated by an electromagnetic method. At an initial density of 0.9–1.2 g/cm^3, the von Neumann spike was either weak or not observed at all. This indicates a fast reaction whose time is outside the experimental resolution (about 5 ns). Electrical conductivity measurements provided only a rather rough upper-bound estimate of the reaction time (less than tens of nanoseconds). Density measurements using synchrotron radiation showed that the initiation of PETN with an air shock wave led to an almost instantaneous initiation of detonation, without an acceleration stage. In general, the results of the study confirm that the chemical reaction rate in ultrafine explosives is increased.

Keywords: detonation, explosion, nanomaterials.

DOI: 10.1134/S0010508221030114

INTRODUCTION

In recent years, there has been interest in ultrafine explosives (UFEs). They have a small critical diameter and a small critical layer thickness. These features suggest a sharp acceleration of the reaction in the wave front due to increased hot-spot density, compared to substances with conventional particle sizes. The prospects of ultrafine explosives have been confirmed in a number of studies [1–3]. However, so far, such studies have mainly focused on the development of technologies for obtaining materials and particle size characterization. Detonation experiments were limited to determining the sensitivity and critical dimensions and measuring detonation velocities, which, for conventional explosives, approximately corresponds to the level of the 1940s. The structure of the detonation wave has not been studied by modern methods.

The lack of data on the structure of detonation waves in UFEs is due to difficulties in producing these materials in quantities sufficient for conventional tests (about 1 kg per experiment with a charge diameter of 60–80 mm) and using electromagnetic sensors with an arm length of about 1 cm. However, under the expected conditions of acceleration of the reaction, the requirements for the charge size are less stringent. Previously, we have developed an electromagnetic technique [4] that allows a sharp reduction in the charge size. When using sensors with a working arm length of $\approx$1 mm, a 20 mm diameter of charges weighing about 10 g is acceptable. The previously developed method of electrical conductivity [5, 6] also allows the use of small charges (several grams). Using these methods, we studied the detonation characteristics of ultrafine PETN and HMX. Experiments confirmed the expected acceleration of the chemical reaction in the detonation wave front.

In addition, we performed experimental studies of the high-enthalpy initiation of PETN by hot gas flow produced by explosion of a small explosive sample. The dynamics of the process was observed using synchrotron

[a]Lavrent'ev Institute of Hydrodynamics, Siberian Branch, Russian Academy of Sciences, Novosibirsk, 630090 Russia; ers@hydro.nsc.ru.
[b]Biysk Oleum Plant, Biysk, 659315 Russia.

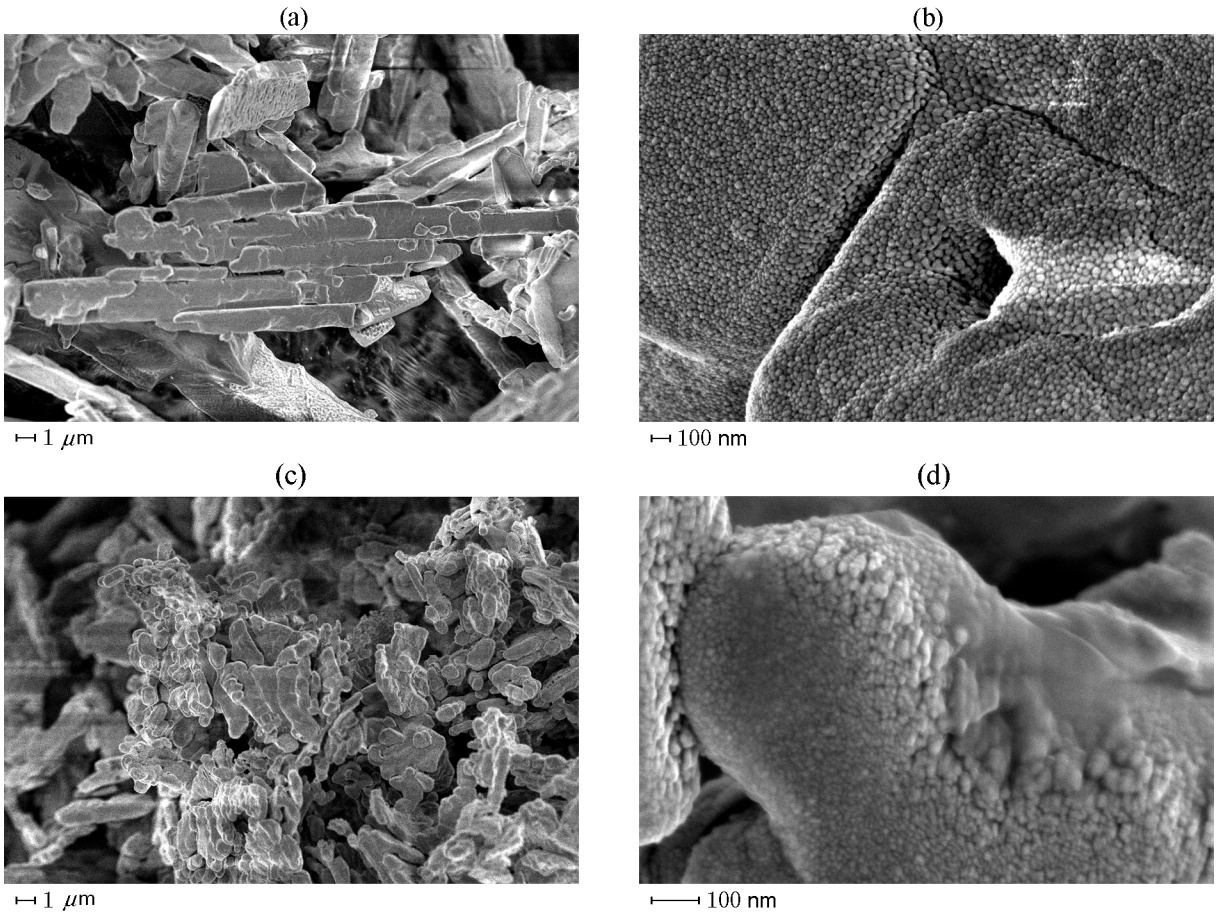

Fig. 1. UFE particles at different magnifications: (a, b) PETN; (c, d) HMX.

radiation beam exposure. Unlike conventional PETN, the detonation of the ultrafine material developed practically instantaneously, without a noticeable acceleration stage.

SAMPLE PREPARATION

Ultrafine PETN with a specific surface area of 10 000–11 000 cm^2/g and ultrafine HMX with a specific surface area of 20 000–21 000 cm^2/g were prepared by crystallization at the Biysk Oleum Plant. The structure of the material is shown in Fig. 1. UFE particles are micron-sized elongated conglomerates of grains with a typical size of tens of nanometers.

Both ultrafine materials were easily electrified and were prone to the formation of lumps and air suspension. Charges were prepared by applying a slight pressure (e.g., a load of about 1 kg for a charge with a diameter of 18 mm). This provided a density of about 0.5 g/cm^3. Higher density values were obtained by pressing in portions. It should be noted that the ultrafine material is much harder to compress and the homogeneity of charges is worse than for materials with conventional particle size. Despite the higher crystal density, HMX under similar loads was compacted to a lower density than PETN.

MEASURING PARTICLE VELOCITY

Electromagnetic diagnostics is described in detail in [4]. UFE were charged into a cylindrical shell 18 mm in inner diameter and about 20 mm long. An aluminum U-shaped sensor 9 μm thick with a working arm length of about 1 mm was placed on a Plexiglas block 8 mm thick, in the plane of the rear face of the charge. For protection, the sensor was coated with an epoxy layer 50–100 μm thick. The UFE charge was initiated from the opposite end using a special small-sized plane-wave generator. A magnetic field $B = 0.15$ T was generated

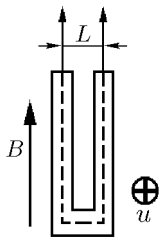

Fig. 2. Shape and effective length of the sensor: the directions of the magnetic induction B and the velocity of the sensor arm u.

by a disposable Helmholtz coil using a current pulse from a capacitor. A thin grounded aluminum electrode was placed upstream and slightly away from the sensor (at 2–3 mm) to eliminate polarization noise. The time resolution was about 5 ns.

Since the width of the connectors (usually 0.4 mm) was comparable to the sensor arm length, the issue of the sensor response was considered. Appendix contains calculations that confirm the intuitive expectation: the sensor operates as a narrow contour, with the effective arm length L being the distance between the midlines of the connectors (Fig. 2).

Time dependences of the velocity of the explosive–Plexiglas interface for two experiments with PETN with a density of 1.0 g/cm^3 are shown in Fig. 3a. The scatter of data due to difficulties in handling UFEs is rather large. Figure 3b shows averaged velocity profiles (each obtained from two experiments) for charges with a density of 1.0 and 1.2 g/cm^3.

The pulse rise time is about 10 ns, which is close to the limiting resolution of the method of 5 ns; the additional broadening can be explained by the inhomogeneity of the explosives. The CJ velocities of the interface were produced by the detonation products from the Chapman–Jouguet states of (determined in [7]) interaction with the Plexiglas window. At a density of 1.0 g/cm^3, the excess of the CJ velocity is rather small (if any), and with an increase in density, it is not observed at all. It can be assumed that in the compacted UFEs, the reaction is so fast that the von Neumann spike becomes almost invisible against the background of the experimental smearing of the profile. The slightly smaller signal amplitude compared to the calculated level in Fig. 3b can be attributed to the error of the calculation as well as to the deviation of the real density of the charge in the region of the sensor from the expected value.

However, at minimum densities at which it is still possible to achieve acceptable homogeneity of the charge, the von Neumann spikes in both PETN and

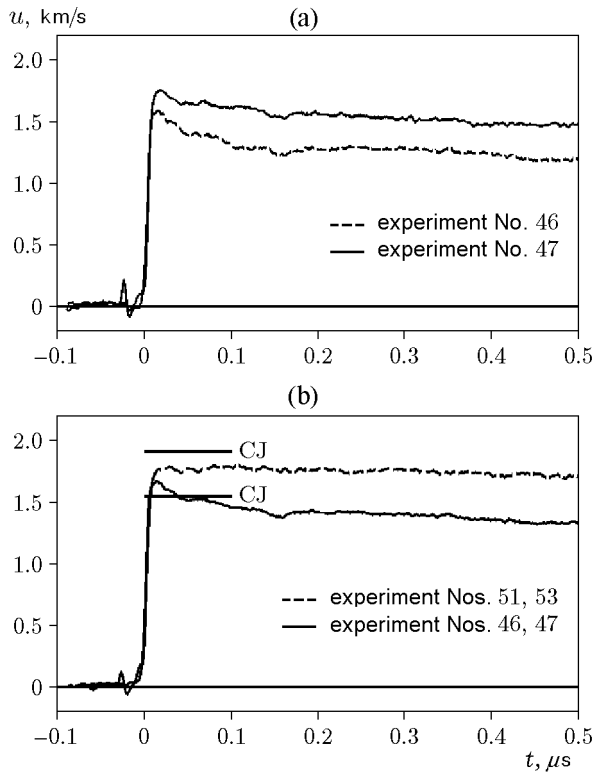

Fig. 3. Velocity profiles at the interface with Plexiglas during detonation of ultrafine PETN: (a) results of two experiments at a density of 1.0 g/cm^3; (b) averaged profiles at densities of 1.0 g/cm^3 (lower curve) and 1.2 g/cm^3 (upper curve); the calculated velocities of the interface for Chapman–Jouguet states are denoted as CJ.

HMX are quite pronounced, as can be seen from Fig. 4a: the velocity in the spike is ≈40% higher than the CJ level. Consequently, with a decrease in the initial density, the reaction time increases and significantly exceeds the resolution of the method. Apparently, under these conditions, the concentration of hot spots decreases, which is discussed in more detail below. With increasing density in HMX, the same picture is observed as in PETN: the von Neumann spike ceases to be visible (Fig. 4b).

ELECTRICAL CONDUCTIVITY PROFILES

Previously, we have performed a comparative study of conventional coarse PETN, RDX, and HMX (particle size of a few hundreds of micrometers) and the same fine-grained explosives (particle size of a few tens of mi-

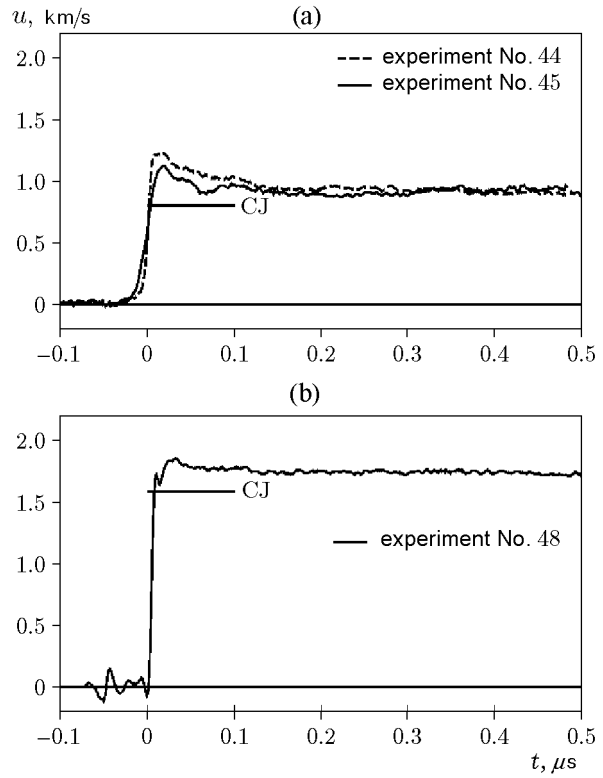

Fig. 4. Detonation velocity profiles: (a) ultrafine PETN (density of 0.51 g/cm^3 in experiment No. 44) and ultrafine HMX (density of 0.47 g/cm^3 in experiment No. 45); (b) ultrafine HMX with a density of 0.94 g/cm^3; the calculated velocities of the interface for Chapman–Jouguet states are denoted as CJ.

crometers) [6, 8]. With almost the same amplitude, the width of the electrical conductivity peak correlating with the chemical reaction zone in fine explosives was approximately half that in coarse ones. Dynamic measurements confirmed a similar reduction in the von Neumann spikes [9]. Therefore, it was of obvious interest to investigate electrical conductivity distributions in the UFEs.

The results of two experiments with PETN and HMX are shown in Fig. 5.

Unfortunately, the above-mentioned inconveniences in handling UFEs affected the quality of the samples in these experiments, which were carried out with charges of small diameter (8 mm) in a thick copper shell. The charges had a distinct density inhomogeneity, which gave rise to a marked scatter of data. Nevertheless, the results can be compared with the data obtained for explosives with a particle size of tens of micrometers [6]. With practically the same density, the amplitude of the peak in ultrafine PETN is on average half that in PETN with a particle

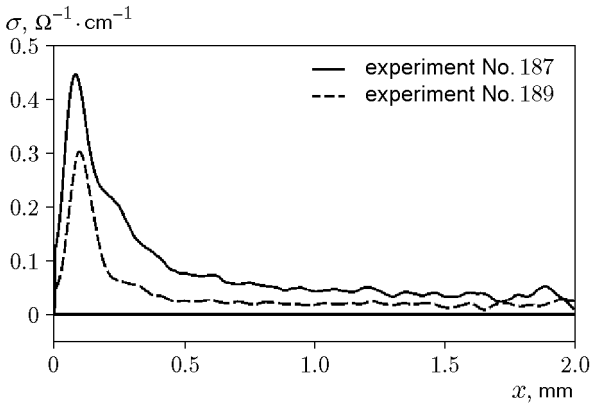

Fig. 5. Electrical conductivity profiles behind the detonation front of UFEs with a density of 1.1 g/cm^3: the upper curve refers to PETN, and the lower curve to HMX.

size of 80 μm. In ultrafine HMX, the peak conductivity is an order of magnitude lower than that in HMX with a particle size of 21 μm. The peak width in both cases did not change markedly and was about 0.2–0.3 mm.

Perhaps, the peaks in ultrafine materials were even narrower, but in these experiments, we, in essence, went beyond the resolution limit of the method. The results can be fitted to the data [6] by assuming a small distortion of the wave front. The measuring cell records electrical conductivity in a fixed plane perpendicular to the charge axis. If the front plane is inclined, e.g., if its normal vector deviates from the axis by an angle $\theta \simeq 1^\circ$, then for a charge diameter $d = 8$ mm, the distortion will increase the peak width by $d\theta \approx 0.14$ mm. Then, the real width of the peak can be 0.06–0.16 mm, i.e., 2–3 times smaller than the measured value. Accordingly, the real amplitude of electrical conductivity will be several times greater than the measured value and will approach the results [6]. According to experience, for ultrafine explosives, good homogeneity of the charge is much more difficult to achieve, and distortions of the wave front due to local density fluctuations are almost inevitable. Thus, the electrical conductivity data do not rule out a very fast reaction (the zone width is less than 0.1 mm, and the time is less than a few nanoseconds).

HIGH-ENTALPY INITIATION OF UFES

The results of studies of detonation initiation of a bulk-density charge of PETN powder by high-enthalpy gas flow are described in [10, 11]. For conventional PETN (particle size of about 0.3 mm), the

initiating flow produced by of the small charge separated by the air gap is filtered into the pores of the charge and simultaneously slightly compacts the powder. With sufficient flow intensity (at a shock wave pressure of about 10 MPa), the reaction starts in the powder and a detonation develops in about 10 μs on a base of about of 20 mm. The most complete data were obtained by the synchrotron radiography. It was natural to apply this experience to study UFEs.

The experimental setup using synchrotron radiation (SR) is described in detail in [11]. In these experiments, we used longitudinal recording: the charge axis was located in the plane of the SR beam, which is similar to optical streak registration. The change in the density of the substance during shock-wave passage influenced the intensity of the radiation transmitted through each cross section and received by a linear multichannel detector.

Figure 6 shows the results of experiments for UFEs and, for comparison, the results for conventional PETN. Charges were placed in plastic shells with an inner diameter of 15 mm. The charges had the lowest possible initial densities at which acceptable homogeneity of the charge was achieved. The exposure parameters were the same for both charges and corresponded to the near-critical initiation of conventional PETN.

There is a sharp difference in the behavior of ultrafine and conventional PETN. In the coarse conventional explosive, the wave is accelerated gradually (the velocity in the initial section is about 0.8 km/s, and at the end of the record, it is 1.25 km/s). This coincides with our previous measurements [11]. In ultrafine PETN, normal detonation with a velocity of 3.8 km/s develops almost instantaneously, and the acceleration region, if any, could not be identified. As expected, the ultrafine material was found to be more active.

At this stage, the mechanism of initiation of UFEs is not clear. One may expect both direct shock-wave action and the development of the reaction according to a two-phase mechanism as in the conventional explosive, but much faster due to the small particle size of the material.

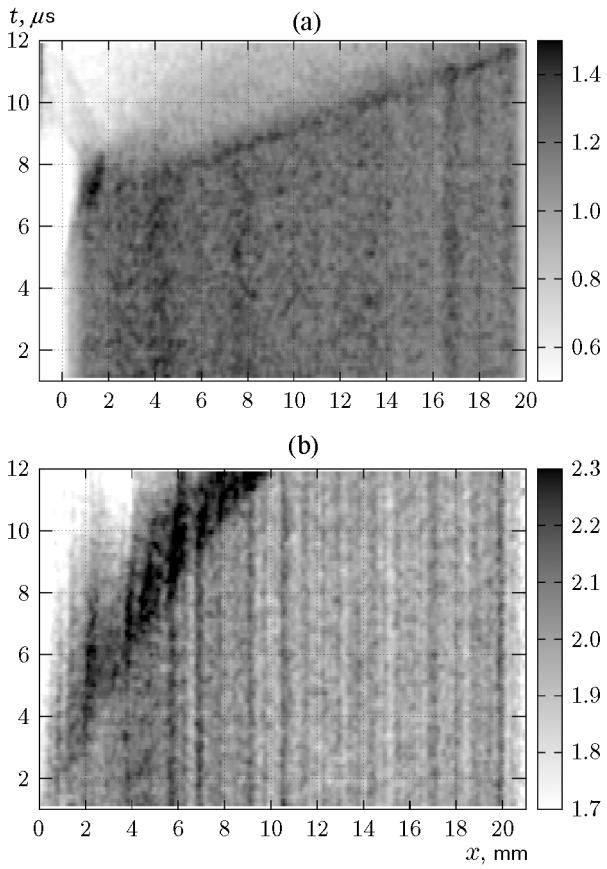

Fig. 6. Streak records of high-enthalpy initiation of detonation: (a) ultrafine PETN (0.5 g/cm^3); (b) conventional PETN (1.0 g/cm^3); the scales on the right is the mass on the ray ρd [g/cm^2].

CONCLUSIONS

Experiments were carried out to determine the detonation parameters of ultrafine explosives. The results indicate a noticeable acceleration of the reaction behind the detonation front in comparison with the same substances with conventional particle sizes. For UFEs compacted to ≈1 g/cm^3 and above, the von Neumann spike was practically invisible in the velocity profiles. Apparently, the reaction occurs in a time less than the resolution of the method (several nanoseconds). This fits into the generally accepted model for the ignition of substances from hot spots, whose density in ultrafine explosives is relatively high. The electrical conductivity data do not contradict this conclusion, given the possibility of distortions of the wave front due to the inhomogeneity of ultrafine materials. The disappearance of the von Neumann spike at relatively low densities was observed earlier [12] in fine RDX (particle size of 5 μm, and density of 1.3 g/cm^3).

In contrast, at low densities (≈0.5 g/cm^3), the reaction slows down and it is possible to observe the von Neumann spike. This can be explained by a decrease in the efficiency of the hot-spot mechanism. Indeed, an initial density of 0.5 g/cm^3 corresponds to a porosity of about 70%. Even at the compression peak, the density increases by a factor of only ≈1.5 and the porosity decreases to 40–50%, i.e., the total pore volume

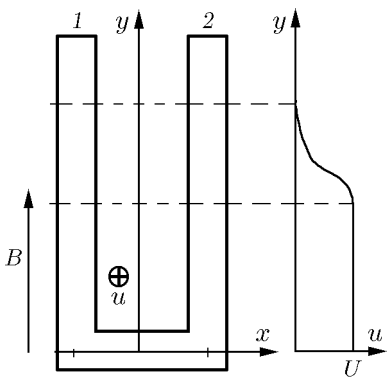

Fig. 7. Calculation geometry.

decreases by less than half. Therefore, sufficient heating is possible only in a small fraction of pores, where significant compression is achieved. Due to a decrease in the concentration of effectively working reaction hot spots, ignition from them takes a longer time. It is possible that a decrease in the speed of combustion propagation from hot spots also plays a role at a relatively low pressure.

During high-enthalpy initiation, detonation in ultrafine explosives

develops much faster than in conventional explosives. This suggests that transient processes critically depend on the particle size of the explosives.

This work was supported by the Russian Foundation for Basic Research (Grant No. 18-03-00441).

APPENDIX

ELECTROMAGNETIC SENSOR RESPONSE

For a small-sized sensor, its conductors cannot be made negligibly narrow for survivability reasons. For example, for a sensor with a total width of

1.4 mm, the width of the connectors was about 0.4 mm. This requires a clear definition of the effective size of the working arm L. If we reason in terms of the change in the magnetic flux through the moving contour, the question arises about the choice of this contour, say, along the outer edge of the sensor or along the inner edge. It was natural to assume that the correct length L corresponds to the midline shown in Fig. 2. This assumption turns out to be quite valid provided that the length of the connectors is large compared to their width s.

Let, initially, the U-shaped sensor be located in the horizontal plane xy, and its crossbar (located at the center of the charge) begins to move in the z direction with velocity U (Fig. 7). The sensor leads are also moving, and their velocity u depends on

the location (y coordinate), so that outside the charge, the velocity vanishes (see the graph on the right in Fig. 7). The magnetic field B is directed along the y axis, parallel to the sensor leads. The current density in the moving conductive material is

$$\boldsymbol{j} \propto Bu\boldsymbol{e}_x - \nabla\varphi,$$

where φ is the electric field potential, $\boldsymbol{e}_x$ is the unit vector in the x direction. From the continuity equation $\nabla \cdot \boldsymbol{j} = 0$, it follows that φ obeys the Laplace equation $\nabla^2\varphi = 0$. At the boundaries of the sensor, the normal component of the current density is zero. As a result, on the vertical (in Fig. 7) boundaries, $\dfrac{\partial\varphi}{\partial x} = Bu$. In the regions of these boundaries where $u \neq 0$, charges occur (positive on the right edges of the leads and negative on the left edges), which form the potential distribution and the signal to be measured.

To eliminate the boundary conditions, we represent the potential φ as

$$\varphi = Bu(y)x + \psi,$$
$$\nabla\varphi = Bu(y)\boldsymbol{e}_x + Bx\frac{du}{dy}\boldsymbol{e}_y + \nabla\psi.$$

Then, throughout the boundary, the normal derivative of ψ is equal to zero (in the region of the crossbar $u = U = \text{const}$, so that the vertical derivative on the crossbar is also zero). The equation for the correction ψ has the form

$$\nabla^2\psi = -Bx\frac{d^2u}{dy^2}; \tag{1}$$

i.e., ψ is generated by the space charge concentrated in the region where the velocity changes. Below this region, $\psi = 0$. We assume that the velocity u changes sharply in a narrow interval at $y = R \ldots R - \varepsilon$ (near the boundary of the charge), and in this interval,

$$\nabla^2\psi \approx \frac{d^2\psi}{dy^2} = -Bx\frac{d^2u}{dy^2}.$$

Then, on this layer, the potential difference is

$$\psi(R) - \psi(R-\varepsilon)$$
$$= -Bx(u(R) - u(R-\varepsilon)) = BUx.$$

Consequently, the value of ψ at the upper boundary of the velocity change interval $\psi(y = R) = BUx$. Since, further, $u = 0$, the potential φ will also have the same value: $\varphi(y = R) = BUx$.

It remains to determine the potential φ at $y > R$. It is the value of the potential at a distance from the

charge boundary where the measuring contacts are attached that determine the sensor readings. Consider the right terminal (*2* in Fig. 7). In the region $y > R$, we have the Laplace equation for φ and the single nonzero condition at the lower boundary:

$$\varphi(x, y = R) = BUx$$
$$= BU\frac{L}{2} + BU\left(x - \frac{L}{2}\right) = BU\frac{L}{2} + BU\xi.$$

The second term determines the variable part of the potential. Decomposing it into the Fourier series on the interval $-s/2 < \xi < s/2$, where s is the width of the conductor, subject to the conditions $\dfrac{\partial\varphi}{\partial\xi} = 0$ for $\xi = \pm s/2$, we obtain

$$BU\xi = BUs\frac{4}{\pi^2}\left(\sin\left(\frac{\pi\xi}{s}\right)\right.$$
$$\left. - \frac{1}{9}\sin\left(\frac{3\pi\xi}{s}\right) + \frac{1}{25}\sin\left(\frac{5\pi\xi}{s}\right) - \ldots\right).$$

The solution of the Laplace equation which decays with increasing y has the form

$$\varphi = BU\frac{L}{2} + BUs\frac{4}{\pi^2}\sum_{k=0}^{\infty}\frac{(-1)^k}{(2k+1)^2}$$
$$\times \sin\left(\frac{(2k+1)\pi\xi}{s}\right)\exp\left(-\frac{(2k+1)\pi(y-R)}{s}\right).$$

The first term in the sum decreases more slowly than the subsequent terms, so that at $y - R \gg s$, we have

$$\varphi = BU\frac{L}{2} + BUs\frac{4}{\pi^2}\sin\left(\frac{\pi\xi}{s}\right)\exp\left(-\frac{\pi(y-R)}{s}\right).$$

For example, at $y - R = 2$ mm and $s = 0.4$ mm, the variable correction is of the order of 10^{-7}, i.e., for reasonable parameter values, the output potential of conductor 2 can be considered equal to $\varphi_2 = BUL/2$. Similarly for conductor 1, $\varphi_1 = -BUL/2$, and the total output voltage $\varphi_2 - \varphi_1 = BUL$.

The above was validated by numerical calculations. Equation (1) was

solved in a rectangular strip, and the velocity $u(y)$ on the decay region was defined by a smooth function with a limited second derivative. The calculations confirmed the analytical asymptotics given above. Thus, the sensor with leads of finite width is equivalent to an infinitely narrow contour as shown in Fig. 2. The error of this approximation decreases exponentially with increasing distance of the contacts from the charge boundary and is always negligible in practice. Note that the effective arm length L should not be significantly larger than the width of the terminals s, and the gap between the terminals can even be practically zero only if there is no closure of the terminals during the motion of the sensor.

REFERENCES

1. A. Ihnen, B. Fuchs, A. Petrock, P. Samuels, V. Stepanov, A. D. Stasio, and W. Lee, "Inkjet Printing of Nanocomposite High-Explosive Materials," in *Proc. of 14th Int. Detonation Symp.*, ONR 351-10-185 (Coeur d'Alene, 2010), pp. 37–40.
2. R. Knepper, M. P. Marquez, and A. S. Tappan, "Effects of Confinement on Detonation Behavior of Vapor-Deposited Hexanitroazobenzene Films," in *Proc. of 15th Int. Detonation Symp.*, ONR 43-280-15 (San Francisco, 2014), pp. 557–565.
3. D. V. Mil'chenko, V. A. Gubachev, L. A. Andreevskikh, S. A. Vakhmistrov, A. L. Mikhailov, V. A. Burnashov, E. V. Khaldeev, A. I. Pyatoikina, S. S. Zhuravlev, and V. N. German, "Nanostructured Explosives Produced by Vapor Deposition. Structure and Explosive Properties," Fiz. Goreniya Vzryva **51** (1), 96–101 (2015) [Combust., Expl., Shock Waves **51** (1), 80–85 (2015); doi.org/10.1134/S0010508215010086].
4. A. P. Ershov and I. A. Rubtsov, "Detonation of Low-Density Explosives," Fiz. Goreniya Vzryva **55** (1), 128–135; DOI: 10.15372/FGV20190113 [Combust., Expl., Shock Waves **55** (1) 114–120 (2019); doi.org/10.1134/S0010508219010131].
5. A. P. Ershov, N. P. Satonkina, and G. M. Ivanov, "Conductivity Profiles in Dense Explosives," Khim. Fiz. **26** (12), 21–33 (2007).
6. A. P. Ershov and N. P. Satonkina, "Electrical Conductivity Distributions in Detonating Low-Density Explosives—Grain Size Effect," Combust. Flame **157** (5), 1022–1026 (2010); DOI: 10.1016/j.combustflame.2009.11.011.
7. K. Tanaka, "Detonation Properties of Condensed Explosives Computed using the Kihara–Hikita–Tanaka Equation of State," Tech. Report (Nat. Chem. Lab. for Industry, Tsukuba Research Center, Tsukuba, 1983).
8. A. P. Ershov and N. P. Satonkina, "Electrical Conductivity Profiles in Detonating Low-Density Explosives of Various Grain Sizes," in *Proc. of 14th Int. Detonation Symp.*, ONR 351-10-185 (Coeur d'Alene, 2010), pp. 302–305.
9. A. P. Ershov, A. O. Kashkarov, E. R. Pruuel, N. P. Satonkina, V. V. Sil'vestrov, A. S. Yunoshev, and A. V. Plastinin, "Nonideal Detonation Regimes in Low Density Explosives," J. Appl. Phys. **119** (7), 075903(1–6) (2016); DOI: 10.1063/1.4942359.
10. L. A. Luk'yanchikov, E. R. Pruuel, A. O. Kashkarov, and K. A. Ten, "Ablation Combustion of Secondary Powder Explosives," Prikl. Mekh. Tekh. Fiz. **51** (4), 5–16 (2010) [J. Appl. Mech. Tech. Phys. **51** (4), 453–462 (2010); doi.org/10.1007/s10808-010-0061-7].

11. A. P. Ershov, A. O. Kashkarov, L. A. Lu'kyanchikov, and E. R. Pruuel, "Initiation of Detonation of a Porous High Explosive by a High-Enthalpy Gas Flow," Fiz. Goreniya Vzryva **49** (1), 91–105 [Combust., Expl., Shock Waves **49** (1), 79–91 (2013); doi.org/10.1134/S0010508213010097].

12. A. V. Utkin, S. A. Kolesnikov, S. V. Pershin, and V. E. Fortov, "Influence of Initial Density on the Reaction Zone for Steady-State Detonation of High Explosives," in *Proc. of 12th Int. Detonation Symp.* (San Diego, 2002), pp. 175–182.